# Generating and Manipulating Higher Order Fano Resonances in Dual-Disk Ring Plasmonic Nanostructures

**Yuan Hsing Fu,* Jing Bo Zhang, Ye Feng Yu, and Boris Luk'yanchuk**

Data Storage Institute, Agency for Science, Technology and Research, DSI Building, 5 Engineering Drive 1, 117608 Singapore

**ABSTRACT**

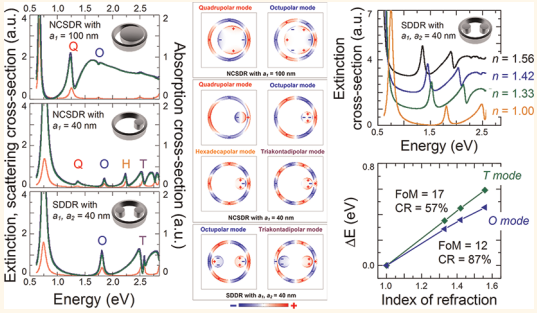


In this article, we investigate higher order (quadrupolar, octupolar, hexadecapolar, and triakontadipolar) Fano resonances generated in disk ring (DR) silver plasmonic nanostructures. We find that the higher order Fano resonances are generated when the size of the disk is reduced and falls into a certain range. With dual-disk ring (DDR) nanostructures, a rich set of tunable Fano line shapes is provided. More specifically, we report our observations on the optical behavior of the DDRs including asymmetric cases either in two disks with different sizes or their asymmetric locations inside the ring. In the case of symmetric dual-disk ring (SDDR) nanostructures, we demonstrate that the quadrupolar and the hexadecapolar Fano resonances are suppressed, which can reduce the cross-talk in spectroscopic measurements, while the octupolar and the triakontadipolar Fano resonances are enhanced. The potential of using the studied plasmonic nanostructures as biochemical sensors is evaluated with the figure of merit (FOM) and the contrast ratio (CR). The values of the FOM and the CR achieved using the triakontadipolar Fano resonance in the SDDR are 17 and 57%, respectively. These results indicate that the SDDRs could be developed into a high-performance biochemical sensor in the visible wavelength range.

**KEYWORDS:** plasmon · Fano resonance · single-disk ring (SDR) · dual-disk ring (DDR) · silver nanostructures · figure of merit · contrast ratio

Fano resonances result from interference of broad and narrow excitation modes, and they are typically more sensitive to changes of the refractive index of the environment.[1] In the past decade, it has been realized that Fano resonances can also be generated in plasmonic nanostructures with relatively easy control. Thus, considerable interest has emerged with many promising applications in physical, chemical, and biological sciences.[1,2] Among the topics related to enhancement of the sensitivity, it was the excitation of the higher order Fano resonances suggested in recent years.[3−11] Such resonances provide good tunability to the Fano line shapes. Among the practical examples, one can mention the disk ring (DR) plasmonic nanostructures,[10−12] where the ring provides the higher order multipolar resonance modes (subradiant modes or narrow dark mode)[13,14] which are coupled with the disk dipolar mode (superradiant mode or broad bright mode). Breaking symmetry by displacing the disk with respect to the ring provides a crucial mechanism for enhancing the coupling of the plasmon modes.[15] Reported results show that the quadrupolar resonance mode is excited at normal incidence while the excitation of the higher order modes (*e.g.*, octupolar and hexadecapolar modes) needs an oblique incidence. By variation of the incident angle, the shape of the Fano resonance can be altered from asymmetric to symmetric. Literature shows that quadrupolar and the octupolar Fano resonances are generated in theta-shaped ring-rod nanostructures[16] and in plasmonic oligomer clusters[8,17−20] at normal incidence. However, the tunability of the Fano line shapes might be limited due to the length of the rod and the size increasing with complex clusters. Our group has recently proposed a silver dual-disk ring (DDR) plasmonic nanostructure to achieve Fano resonance in the visible wavelength range,[21] resulting from the coupling of higher order modes, that is, coupling of the ring octupolar mode and disk dipolar mode.

In this article, we investigate the generation of higher order Fano resonances in different nanostructures. We find that the higher order Fano resonances can be generated when the size of the disk is reduced and falls into a certain range, where the quadrupolar, octupolar, hexadecapolar, and triakontadipolar Fano resonances appear.

* Address correspondence to fu_yuan_hsing@dsi.a-star.edu.sg.

Received for review February 22, 2012 and accepted May 11, 2012.

**Published online May 11, 2012**
**10.1021/nn3007898**

The Fano line shapes are tuned by changing the geometric parameters of an individual disk in the DDR plasmonic nanostructures. To our knowledge, the current work reports the first study of asymmetric dual-disk ring (ADDR) nanostructures where the "asymmetry" is either in two disks with different sizes or their asymmetric locations inside the ring. With the symmetric dual-disk ring (SDDR) nanostructures, we demonstrate that the quadrupolar and the hexadecapolar Fano resonances are suppressed, which can reduce the cross-talk in spectroscopic measurements, while the octupolar and the triakontadipolar Fano resonances are enhanced. The potential of using such plasmonic nanostructures as biochemical sensors is evaluated with values of the figure of merit (FOM)[22,23] and the contrast ratio (CR).[24]

## RESULTS AND DISCUSSION

To start the spectroscopic investigation of both SDR and DDR plasmonic nanostructures, Figure 1 illustrates the geometries considered in this work. The material used in all of the plasmonic nanostructures is silver, a weakly dissipating material.[25] The thickness of the metal layer is $h$. We define the ring structure whose geometric parameters are shown in Figure 1a. The inner and the outer radius of the ring are $r_i$ and $r_o$, respectively. The single-disk or the dual-disk nanostructure is located inside the ring. In the case of a single-disk ring (SDR) nanostructure, if the disk and the ring are concentric, it is referred to as a concentric single-disk ring (CSDR), where $a_1$ is the radius of the disk, as shown in Figure 1b. Symmetry is broken when induced by an offset of the disk with respect to the center of the ring forming a nanogap $g_1$ between the disk and the ring. This asymmetric structure is referred to here as a nonconcentric single-disk ring (NCSDR),[10] as shown in Figure 1c. The dual-disk ring (DDR) nanostructure shown in Figure 1d consists of two disks inside the ring where the radii of the disks are $a_1$ and $a_2$. The $g_1$ and $g_2$ are the respective nanogaps between the disks and the ring. With this, we define two types of DDR nanostructures, a symmetric dual-disk ring (SDDR) and an asymmetric dual-disk ring (ADDR). The SDDR means $a_1 = a_2$ and $g_1 = g_2$, and the ADDR means either $a_1 \neq a_2$ or $g_1 \neq g_2$. The electromagnetic (EM) wave is assumed as normal incidence with the polarization parallel to the gap. Here, we fix the inner and the outer radius of the ring structure ($r_i$ = 130 nm, $r_o$ = 150 nm), the thickness of metal layer ($h$ = 60 nm), and one nanogap $g_1$ = 10 nm, and we change the parameters of $a_1$, $a_2$, and $g_2$ in each nanostructure to study their influences on the generation of Fano resonances and the manipulation of the Fano line shapes.

Figure 2 shows the optical properties of the plasmonic nanostructures considered. We plot both the scattering (green curve) and the absorption (light red curve) spectra of each plasmonic nanostructure to compare the super-radiant and the subradiant plasmon resonance modes and the Fano resonance arising from their interferences.[17] The extinction (dark blue curve) spectra can be easily obtained from the sum of the scattering and the absorption spectra. According to the relationship of the peak positions between the scattering and the absorption, it is easy to determine whether the Fano line shape is symmetric or not. The absorption is related to the near-field enhancement by the subradiant mode and therefore reveals the actual position of the resonance.[26] We compare the spectra of the ring structure (Figure 2a) and the disk with various radii $a_1$ from 120 to 40 nm (Figure 2b–f). The dipolar ring mode at 0.78 eV and dipolar disk modes at 1.51, 1.68, 1.99, 2.46, and 2.81 eV of the disks with the radii of 120, 100, 80, 60, and 40 nm are clearly observed, respectively. The ring mode is narrower than the disk mode, which implies the ring mode and dipolar disk mode are subradiant and super-radiant, respectively.

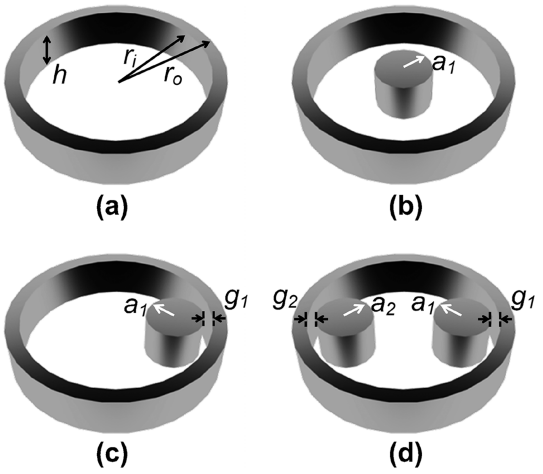


**Figure 1. Schematics of various silver disk ring plasmonic nanostructures under consideration: (a) ring structure with fixed geometric parameters, $r_i$ = 130 nm, $r_o$ = 150 nm, and $h$ = 60 nm; (b) concentric single-disk ring (CSDR) structure consists of the ring and a single-disk with variable radius $a_1$ from 100 to 40 nm; (c) nonconcentric single-disk ring (NCSDR) structure with nanogap $g_1$ = 10 nm and variable radius of disk $a_1$ from 100 to 40 nm; and (d) dual-disk ring (DDR) structure consists of the ring and two disks with radii of $a_1$ and $a_2$. Symmetric dual-disk ring (SDDR) means $a_1 = a_2$ and $g_1 = g_2$, while asymmetric dual-disk ring (ADDR) means either $a_1 \neq a_2$ or $g_1 \neq g_2$.**

Similar scattering and absorption spectra of the CSDR plasmonic nanostructures with various $a_1$ from 120 to 40 nm are shown in Figure 2g–k. The results show that the combined system contains two modes generated by the hybridization of individual disk and the ring dipolar plasmons. From Figure 2h–k, we find that the strength of the absorption peak of the bonding combination of the bonding dipolar and dipolar disk plasmon mode at 0.75 eV reduces from strong to weak coupling. In Figure 2g, a high order resonance peak at 2.44 eV of the CSDR is observed. A similar

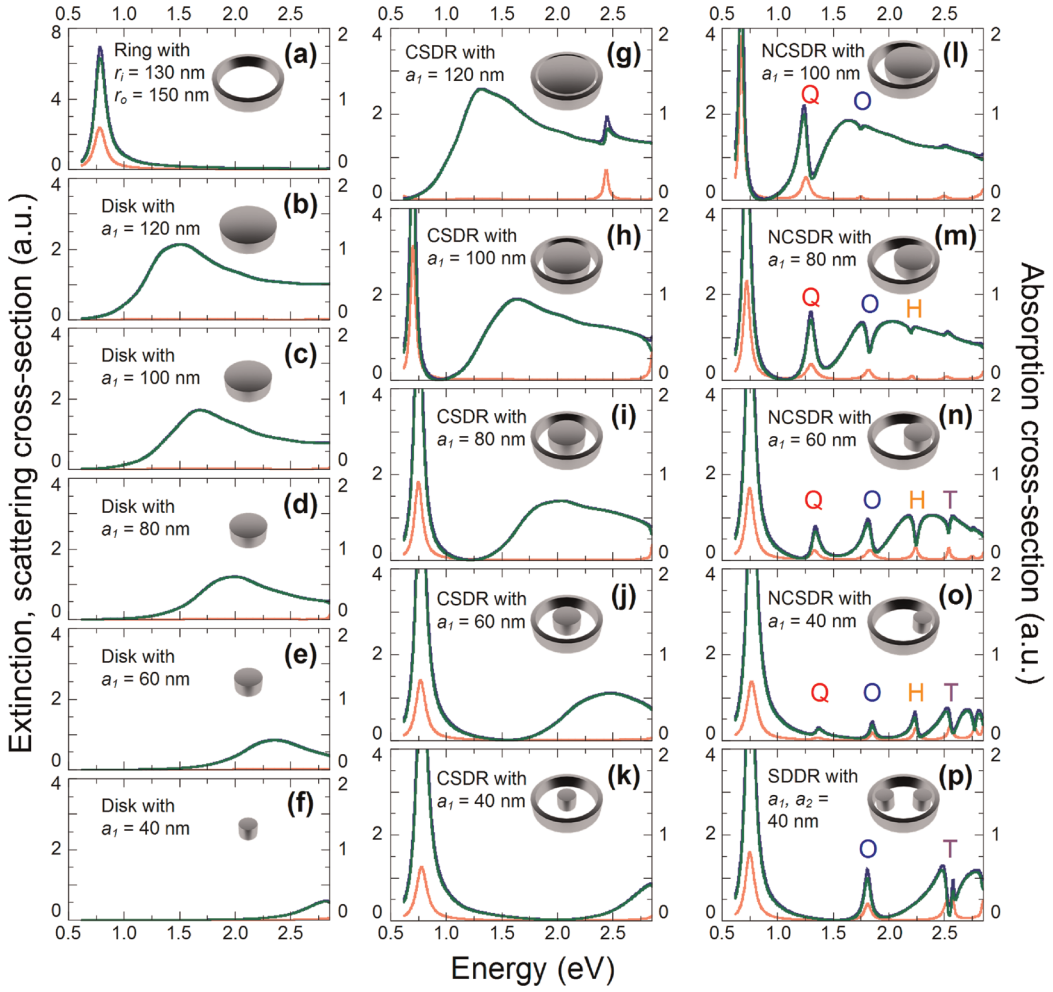


**Figure 2. Extinction (dark blue curve), scattering (green curve), and absorption (light red curve) spectra of (a) ring with $r_i$ = 130 nm and $r_o$ = 150 nm, (b–f) disks with various $a_1$ from 120 to 40 nm, (g–k) concentric single-disk ring (CSDR) plasmonic nanostructures with various $a_1$ from 120 to 40 nm, (l–o) nonconcentric single-disk ring (NCSDR) plasmonic nanostructures with fixed $g_1$ = 10 nm and various $a_1$ from 100 to 40 nm, and (p) symmetric dual-disk ring (SDDR) plasmonic nanostructure with $g_1 = g_2$ = 10 nm and $a_1 = a_2$ = 40 nm. Left and right axes are scattering and absorption, respectively, in each plot. The letters "Q", "O", "H", and "T" represent quadrupolar, octupolar, hexadecapolar, and triakontadipolar Fano resonances, respectively.**

resonance peak is observed in a strongly interacting disk ring silver structure with the thickness of 50 nm.[27]

Figure 2l–o shows the scattering and absorption spectra of the NCSDR plasmonic nanostructures with various $a_1$ from 100 to 40 nm and a fixed nanogap $g_1$ at 10 nm. Fano resonance in Figure 2l at 1.25 eV results from the coupling of the quadrupolar ring mode and the super-radiant disk mode; compare Figure 2l with Figure 2h. The position of the absorption peak at 1.25 eV is different from that of the scattering peak at 1.24 eV, which implies asymmetric Fano line shape. The Fano resonance *via* the quadrupolar ring mode is clearly observed in the charge distribution of the NCSDR, as shown in Figure 3a. The Fano resonance *via* octupolar ring mode also appears at 1.75 eV, as shown in Figure 2l, and the corresponding charge distribution is shown in Figure 3b. However, this octupolar Fano resonance mode is much weaker in comparison with the quadrupolar mode. From Figure 2l–o, more absorption peaks are observed when the size of the disk is reduced, which indicates the excitation of the higher order Fano resonance modes. When the radius of the disk is reduced to 40 nm (Figure 2o), the quadrupolar, octupolar, hexadecapolar, and triakontadipolar Fano resonance modes are found at 1.37, 1.85, 2.24, and 2.55 eV. Their corresponding charge distributions are shown in Figure 3c–f, respectively. Though the strength of the resonance peak becomes lower and lower, the sharp line shape of the higher order Fano resonance mode may be useful for applications where a high sensitivity is required.

Figure 2p is the result of the SDDR plasmonic nanostructure with $a_1 = a_2$ = 40 nm and $g_1 = g_2$ = 10 nm. The resonance peaks occur at 1.81 and 2.53 eV. From the corresponding charge distributions of the SDDR shown in Figure 3g,h, the resonance modes at 1.81 and 2.53 eV are the octupolar and the triakontadipolar Fano resonances, respectively. Comparing the spectra in Figure 2o,p, we find that the SDDR is able to

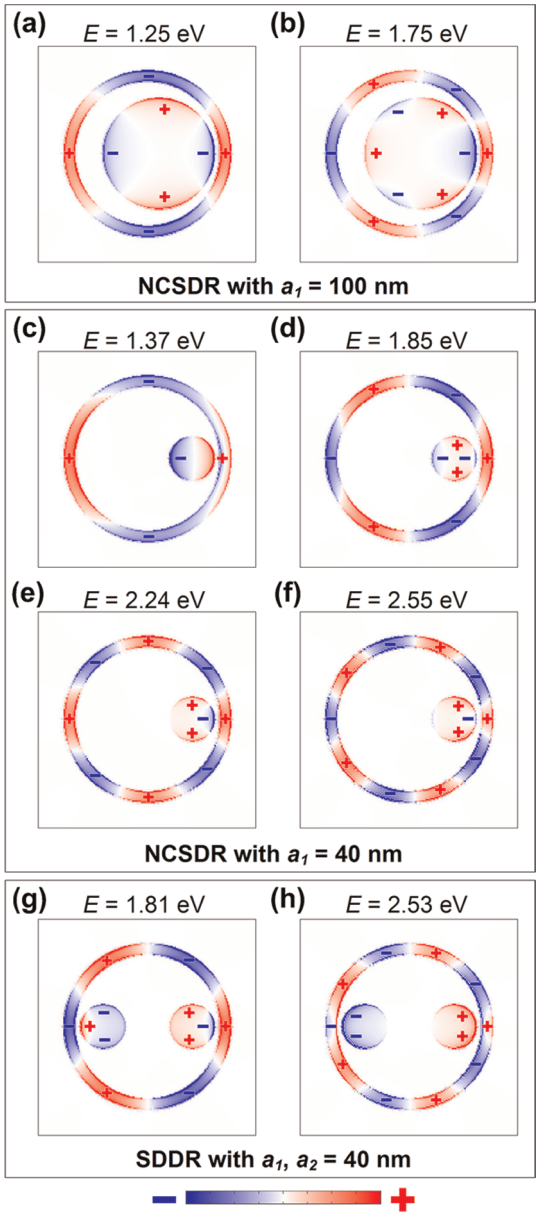


**Figure 3. Charge density distributions of the Fano resonances of (a,b) nonconcentric single-disk ring (NCSDR) structure with $a_1$ = 100 nm and $g_1$ = 10 nm at energies of 1.25 and 1.75 eV, respectively, (c–f) NCSDR structure with $a_1$ = 40 nm and $g_1$ = 10 nm at energies of 1.37, 1.85, 2.24, and 2.55 eV, respectively, and (g,h) symmetric dual-disk ring (SDDR) structure with $a_1 = a_2$ = 40 nm and $g_1 = g_2$ = 10 nm at energies of 1.81 and 2.53 eV, respectively. The signs "+" and "–" represent the positive and negative charges, respectively.**

suppress the quadrupolar and the hexadecapolar Fano resonances and enhance the octupolar and the triakontadipolar Fano resonances to achieve higher order Fano resonances. The two-dip-like shape occurs around 2.5 eV because a resonance peak overlaps the Fano resonance (see Supporting Information Figure S1).

The charge distributions of the NCSDR with $a_1$ = 40 nm (Figure 3c–f) are compared with the SDDR with $a_1 = a_2$ = 40 nm (Figure 3g,h). In Figure 3c–f, the charge distributions on the ring exhibit 4, 6, 8, and 10 nodes, as expected corresponding to quadrupolar, octupolar, hexadecapolar, and triakontadipolar Fano resonances, respectively. The small single disk inside the ring plays a role as a dipole excited by the incident EM wave, and then the dipole induces the excitation of multipolar dark ring modes due to near-field coupling. The multipolar ring modes coupling with the broad dipolar disk mode generate the higher order Fano resonances. For the quadrupolar and the hexadecapolar Fano resonances, the charges on the left and the right sides of the ring have the same sign; for the octupolar and the triakontadipolar Fano resonances, they have opposite signs.

In Figure 3g,h, the two disks oscillate in the same phase. Hence, only the resonance modes with opposite signs of charges on the left and the right sides of the ring are able to exist, as expected, corresponding to the octupolar and the triakontadipolar Fano resonances. Meanwhile, these Fano resonances are enhanced using the symmetric dual-disk.

Figure 4 shows the tunability of the DDR plasmonic nanostructures. In Figure 4a–d, the chosen variable is one of the nanogaps $g_2$ between one disk and the ring, while other parameters, including the radius of the two disks ($a_1 = a_2$ = 40 nm) and the other nanogap ($g_1$ = 10 nm), remain constant. From Figure 4a–d, the DDRs from the ADDRs become the SDDR. The quadrupolar Fano resonance at 1.37 eV and the hexadecapolar Fano resonance at 2.24 eV are suppressed when the gap $g_2$ is reduced. These results demonstrate the suppression of the quadrupolar and the hexadecapolar Fano resonances in SDDR plasmonic nanostructures.

In Figure 4e–h, the two nanogaps are fixed ($g_1 = g_2$ = 10 nm), while the radii of the two disks ($a_1 = a_2$) are changed simultaneously. In Figure 4e,f, the two disks are overlapped and form CSDR-like structures. The feature of the spectra is similar to the spectrum of the CSDR with $a_1$ = 120 nm, as shown in Figure 2g, but a small resonance dip appears around 1.75 eV, as shown in Figure 4e,f. In Figure 4d,g,h, the octupolar Fano resonances in the scattering spectra lead to a symmetric peak in Figure 4d and an asymmetric peak in Figure 4h, and finding a symmetric dip in Figure 4g, when the sizes of the disk are 40, 50, and 57.5 nm, respectively. These different asymmetries due to the relative phase between two interfering modes determines the conditions of destructive and constructive interferences.[28] In Figure 4d, the Fano resonance is highly detuned from the superradiant peak position, resulting in a very high asymmetry parameter and a Lorentzian-like line shape. In Figure 4g, the asymmetry is almost zero as the Fano resonance is almost centered. The intermediate situation of Figure 4h displays an asymmetry.

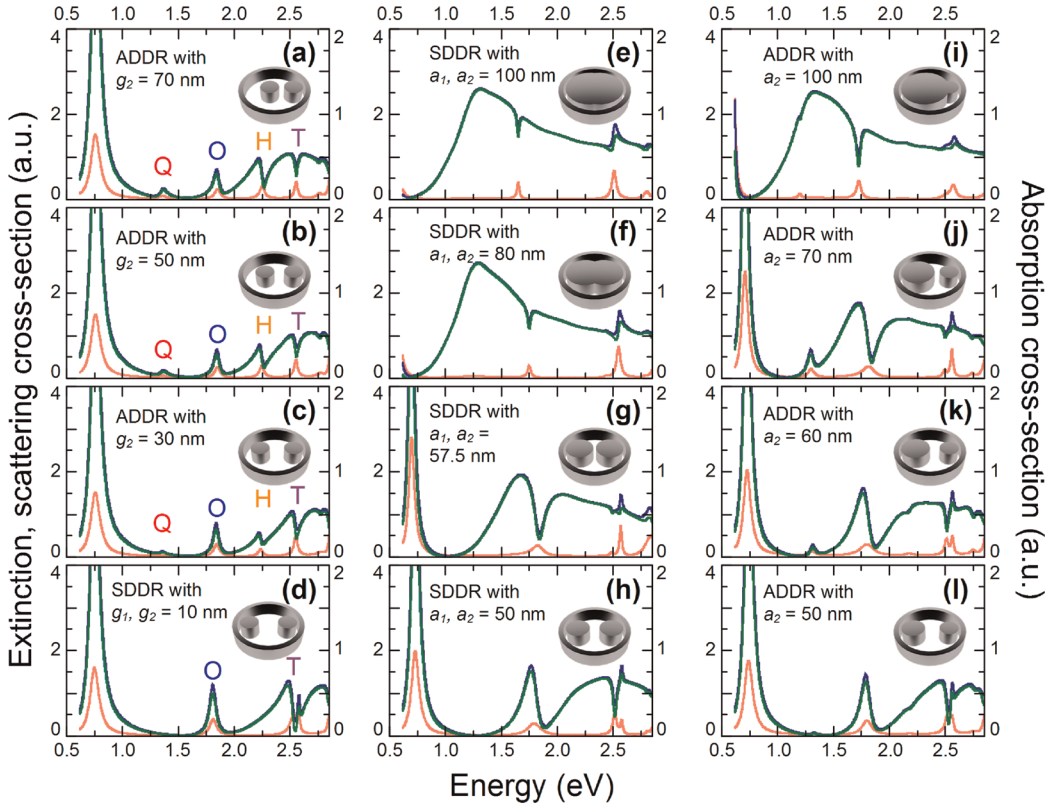


**Figure 4. Extinction (dark blue curve), scattering (green curve), and absorption (light red curve) spectra of (a–c) asymmetric dual-disk ring (ADDR) structures with fixed $a_1 = a_2 = 40$ nm, $g_1 = 10$ nm, and various $g_2$ from 70 to 30 nm; (d) symmetric dual-disk ring (SDDR) structure with $a_1 = a_2 = 40$ nm and $g_1 = g_2 = 10$ nm; (e–h) SDDRs with fixed $g_1 = g_2 = 10$ nm and various $a_1 = a_2$ from 100 to 50 nm; and (i–l) ADDRs with fixed $g_1 = g_2 = 10$ nm, $a_1 = 40$ nm, and various $a_2$ from 100 to 50 nm. Left and right axes are scattering and absorption, respectively, in each plot. The letters "Q", "O", "H", and "T" represent quadrupolar, octupolar, hexadecapolar, and triakontadipolar Fano resonances, respectively.**

In Figure 4i–l, the chosen variable is the radius of one of the disks $a_2$, while the two nanogaps and the radius of the other disk remain constant ($g_1 = g_2 =$ 10 nm, $a_1 = 40$ nm). Due to asymmetry, the quadrupolar and the hexadecapolar Fano resonances appear. In Figure 4i, the two disks are overlapped and form a CSDR-like structure. Compared to Figure 4e,f, the highly asymmetric disk inside the ring leads to a stronger octupolar Fano resonance at 1.73 eV.

To show that a higher order Fano resonance provides higher sensitivity, we use the figure of merit (FOM) and the contrast ratio (CR) to evaluate the performance of the plasmonic nanostructures as biochemical sensors. The FOM is defined as the ratio of the sensitivity to the bandwidth of the resonance [(eV RIU$^{-1}$)/bandwidth]. In the symmetric Fano resonance, the bandwidth is the full width at half-maximum (fwhm) of the resonance, and in the asymmetric Fano resonance, the bandwidth is the line width from the peak to the dip of the resonance.[10,29] The CR is defined as the ratio of the difference between the peak value and the dip value to the sum of these two values. We compare the sensing performance of three plasmonic nanostructures: NCSDR with $a_1 = 100$ nm, CSDR with $a_1 = 120$ nm, and SDDR with $a_1 = a_2 =$ 40 nm. Figure 5a–c shows the spectra of the plasmonic nanostructures with complete dielectric filling (vacuum or dielectrics occupies the semi-filling space over the nanostructure on the glass substrate) of different media ($n$ = 1, 1.33, 1.42, and 1.56). The spectra clearly show significant red shifts with the increase of the refractive index of the surround media. The energy shift dependence on the refractive index is shown in Figure 5d–f. In the structure of the NCSDR (Figure 5a,d), the sensitivity of the quadrupolar Fano resonance (Q mode, at 1.25 eV) is 0.61 eV RIU$^{-1}$. The calculated values of the FOM and the CR are 10 and 68%, respectively. In the structure of the CSDR (Figure 5b,e), the sensitivity of the high order resonance peak (at 2.44 eV) is 1.28 eV RIU$^{-1}$. The calculated values of the FOM can reach 30; however, the CR is only 12%. In the structure of the SDDR (Figure 5c,f), there are two Fano resonances, the octupolar Fano resonance (O mode, at 1.81 eV) and the triakontadipolar Fano resonance (T mode, at 2.53 eV). The sensitivity, the FOM, and the CR of the O mode are 0.84 eV RIU$^{-1}$, 12, and 87%, respectively, while the corresponding values of the T mode are 1.06 eV RIU$^{-1}$, 17, and 57%, respectively. It clearly

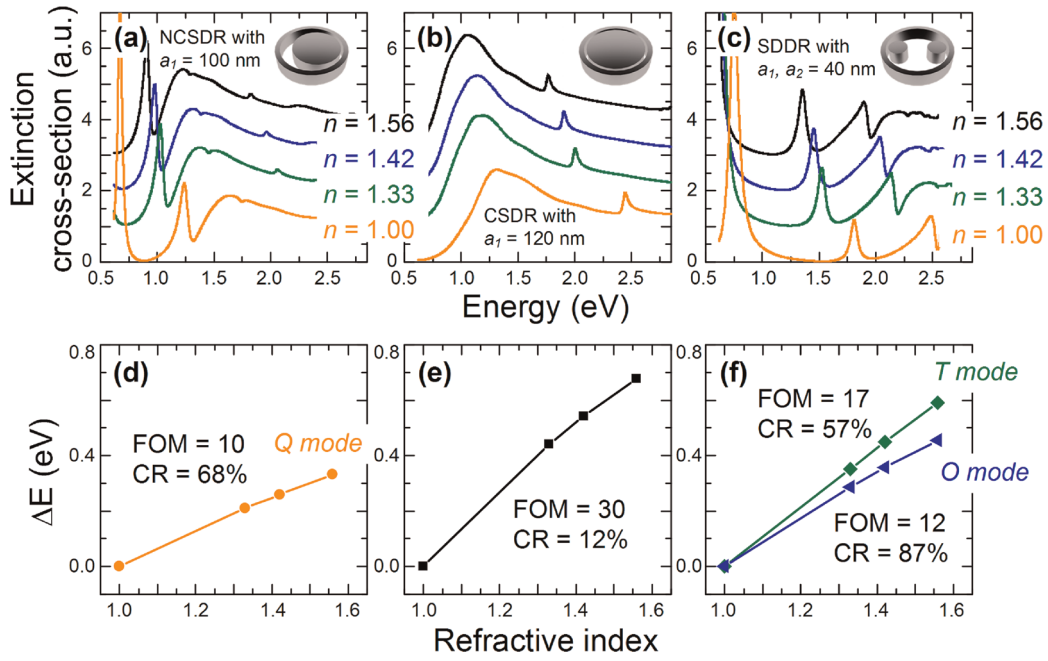


**Figure 5. Extinction spectra of (a) nonconcentric single-disk ring (NCSDR) structure with $a_1$ = 100 nm, (b) concentric single-disk ring (CSDR) structure with $a_1$ = 120 nm, and (c) symmetric dual-disk ring structure with $a_1 = a_2 = 40$ nm for the surrounding media with refractive index at $n$ = 1.00, 1.33, 1.42, and 1.56. (d–f) Energy shifts of the resonances as a function of the refractive index $n$ with (d) quadrupolar Fano resonance (Q mode, at 1.25 eV in 5a), (e) high order resonance peak (at 2.5 eV in panel b), and (f) octupolar (O mode, at 1.81 eV in panel c) and the triakontadipolar (T mode, at 2.53 eV in panel c) Fano resonance. The corresponding values of the figure of merit (FOM) and contrast ratio (CR) are shown in the plots.**

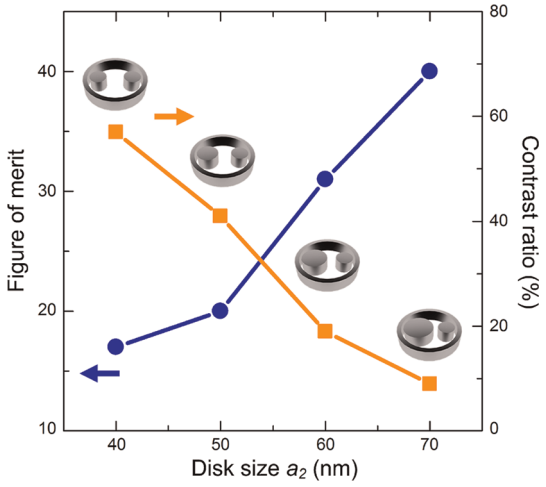


**Figure 6. Figure of merit (dark blue curve) and the contrast ratio (lighter orange curve) using triakontadipolar Fano resonances in the dual-disk ring (DDR) with fixed $a_1$ = 40 nm as a function of the size of the disk $a_2$ from 40 to 70 nm.**

demonstrates that the sensitivity of such biochemical sensor is enhanced with higher order Fano resonance in the case of SDDR plasmonic structure. The FOM value is close to a reported result, 12–20, using a silver nanocube on high refractive index substrate of ZnSe.[30] In addition, the suppression of the quadrupolar and the hexadecapolar Fano resonances can reduce the cross-talk. Similar calculations have been performed (see Supporting Information Figure S2).

We consider the variation of the size of the disk $a_2$ affects the FOM and the CR in the ADDRs. Figure 6 shows the values of the FOM (dark blue curve) and the CR (lighter orange curve) using the triakontadipolar Fano resonances in the dual-disk ring (DDR) nanostructures with fixed $a_1$ = 40 nm as a function of $a_2$ from 40 to 70 nm. The values of the FOM and the CR of the SDDR with $a_1 = a_2 = 40$ nm are 17 and 57%, respectively. The value of the FOM increases when $a_2$ is increased. However, the value of the CR decreases on the one hand. On the other hand, the appearance of the quadrupolar and the hexadecapolar Fano resonances increases the cross-talk in spectroscopic measurements.

## CONCLUSION

In this article, we have systematically studied the generation of the higher order Fano resonances from normal excitation of both single-disk ring (SDR) and dual-disk ring (DDR) silver plasmonic nanostructures. For each type, we vary several geometrical parameters of both symmetric and asymmetric structures to represent most plasmonic nanostructures. We have found that quadrupolar, octupolar, hexadecapolar, and triakontadipolar Fano resonances appear when the size of the disk is reduced and fallen into a certain range. We have demonstrated that the quadrupolar and the hexadecapolar Fano resonances are suppressed while the octupolar and the triakontadipolar Fano

resonances are enhanced in the case of the symmetric dual-disk ring (SDDR) plasmonic nanostructure. Meanwhile, results show large spectral tunability in dual-disk ring (DDR) which provides a rich set of the Fano line shapes. By optimizing the SDDR plasmonic nanostructure, we show that the FOM and the CR using the triakontadipolar Fano resonance are able to reach 17 and 57%, respectively. Additionally, the suppression of the quadrupolar and the hexadecapolar modes can reduce the cross-talk in spectroscopic measurements. The work reports the first study of the asymmetric dual-disk ring (ADDR) plasmonic nanostructures. We hope this article can serve as a template for design and analysis of optical behaviors of plasmonic nanostructures and nanochip-based biochemical sensors.

## METHODS

The scattering and the absorption cross-section spectra of the plasmonic nanostructures were calculated using finite difference time domain (FDTD, Lumerical FDTD Solutions) method. The dielectric function of silver used for calculation was obtained from the experimental data of Johnson and Christy.[31] In all calculation models, the nanostructure lies on a glass substrate ($SiO_2$ with reflective index of 1.456 at wavelength of 656 nm), which occupies semi-filling space under the nanostructure. The charge density distributions were numerically calculated as the divergence of the calculated electric field.

*Conflict of Interest:* The authors declare no competing financial interest.

*Acknowledgment.* The authors acknowledge the finical support by Science and Engineering Research Council (SERC) Grant No. 102 152 0018, and Joint Council (JC) Grant JCOAG03-FG04-2009 of Agency for Science, Technology and Research (A*STAR).

*Supporting Information Available:* The information related to the spectra as a function of the thickness of the SDDR, the similar calculations of values of the FOM and the CR for various SDDR and ADDRs, and the spectra of NCSDRs and SDDRs of using gold. This material is available free of charge *via* the Internet at http://pubs.acs.org.

## REFERENCES AND NOTES

1. Luk'yanchuk, B.; Zheludev, N. I.; Maier, S. A.; Halas, N. J.; Nordlander, P.; Giessen, H.; Chong, C. T. The Fano Resonance in Plasmonic Nanostructures and Metamaterials. *Nat. Mater.* **2010**, *9*, 707–715.
2. Miroshnichenko, A. E.; Flach, S.; Kivshar, Y. S. Fano Resonances in Nanoscale Structures. *Rev. Mod. Phys.* **2010**, *82*, 2257–2298.
3. Bao, K.; Mirin, N. A.; Nordlander, P. Fano Resonances in Planar Silver Nanosphere Clusters. *Appl. Phys. A: Mater. Sci. Process.* **2010**, *100*, 333–339.
4. Artar, A.; Yanik, A. A.; Altug, H. Directional Double Fano Resonances in Plasmonic Hetero-oligomers. *Nano Lett.* **2011**, *11*, 3694–3700.
5. Liu, N.; Hentschel, M.; Weiss, T.; Alivisatos, A. P.; Giessen, H. Three-Dimensional Plasmon Rulers. *Science* **2011**, *332*, 1407–1410.
6. Artar, A.; Yanik, A. A.; Altug, H. Multispectral Plasmon Induced Transparency in Coupled Meta-Atoms. *Nano Lett.* **2011**, *11*, 1685–1689.
7. Liu, N.; Mukherjee, S.; Bao, K.; Brown, L. V.; Dorfmuller, J.; Nordlander, P.; Halas, N. J. Magnetic Plasmon Formation and Propagation in Artificial Aromatic Molecules. *Nano Lett.* **2012**, *12*, 364–369.
8. Dregely, D.; Hentschel, M.; Giessen, H. Excitation and Tuning of Higher-Order Fano Resonances in Plasmonic Oligomer Clusters. *ACS Nano* **2011**, *5*, 8202–8211.
9. Fang, Z.; Cai, J.; Yan, Z.; Nordlander, P.; Halas, N. J.; Zhu, X. Removing a Wedge from a Metallic Nanodisk Reveals a Fano Resonance. *Nano Lett.* **2011**, *11*, 4475–4479.
10. Hao, F.; Sonnefraud, Y.; Van Dorpe, P.; Maier, S. A.; Halas, N. J.; Nordlander, P. Symmetry Breaking in Plasmonic Nanocavities: Subradiant LSPR Sensing and a Tunable Fano Resonance. *Nano Lett.* **2008**, *8*, 3983–3988.
11. Hao, F.; Nordlander, P.; Sonnefraud, Y.; Van Dorpe, P.; Maier, S. A. Tunability of Subradiant Dipolar and Fano-Type Plasmon Resonances in Metallic Ring/Disk Cavities: Implications for Nanoscale Optical Sensing. *ACS Nano* **2009**, *3*, 643–652.
12. Sonnefraud, Y.; Verellen, N.; Sobhani, H.; Vandenbosch, G. A. E.; Moshchalkov, V. V.; Van Dorpe, P.; Nordlander, P.; Maier, S. A. Experimental Realization of Subradiant, Superradiant, and Fano Resonances in Ring/Disk Plasmonic Nanocavities. *ACS Nano* **2010**, *4*, 1664–1670.
13. Hao, F.; Larsson, E. M.; Ali, T. A.; Sutherland, D. S.; Nordlander, P. Shedding Light on Dark Plasmons in Gold Nanorings. *Chem. Phys. Lett.* **2008**, *458*, 262–266.
14. Nordlander, P. The Ring: A Leitmotif in Plasmonics. *ACS Nano* **2009**, *3*, 488–492.
15. Verellen, N.; Sonnefraud, Y.; Sobhani, H.; Hao, F.; Moshchalkov, V. V.; Van Dorpe, P.; Nordlander, P.; Maier, S. A. Fano Resonances in Individual Coherent Plasmonic Nanocavities. *Nano Lett.* **2009**, *9*, 1663–1667.
16. Habteyes, T. G.; Dhuey, S.; Cabrini, S.; Schuck, P. J.; Leone, S. R. Theta-Shaped Plasmonic Nanostructures: Bringing "Dark" Multipole Plasmon Resonances into Action *via* Conductive Coupling. *Nano Lett.* **2011**, *11*, 1819–1825.
17. Mirin, N. A.; Bao, K.; Nordlander, P. Fano Resonances in Plasmonic Nanoparticle Aggregates. *J. Phys. Chem. A* **2009**, *113*, 4028–4034.
18. Rahmani, M.; Lukiyanchuk, B.; Tahmasebi, T.; Lin, Y.; Liew, T.; Hong, M. Polarization-Controlled Spatial Localization of Near-Field Energy in Planar Symmetric Coupled Oligomers. *Appl. Phys. A: Mater. Sci. Process.* **2012**, *107*, 23–30.
19. Rahmani, M.; Lukiyanchuk, B.; Nguyen, T. T. V.; Tahmasebi, T.; Lin, Y.; Liew, T. Y. F.; Hong, M. H. Influence of Symmetry Breaking in Pentamers on Fano Resonance and Near-Field Energy Localization. *Opt. Mater. Express* **2011**, *1*, 1409–1415.
20. Rahmani, M.; Tahmasebi, T.; Lin, Y.; Lukiyanchuk, B.; Liew, T. Y. F.; Hong, M. H. Influence of Plasmon Destructive Interferences on Optical Properties of Gold Planar Quadrumers. *Nanotechnology* **2011**, *22*, 245204.
21. Niu, L. F.; Zhang, J. B.; Fu, Y. H.; Kulkarni, S.; Luky'anchuk, B. Fano Resonance in Dual-Disk Ring Plasmonic Nanostructures. *Opt. Express* **2011**, *19*, 22974–22981.
22. Sherry, L. J.; Chang, S. H.; Schatz, G. C.; Van Duyne, R. P.; Wiley, B. J.; Xia, Y. N. Localized Surface Plasmon Resonance Spectroscopy of Single Silver Nanocubes. *Nano Lett.* **2005**, *5*, 2034–2038.
23. Lassiter, J. B.; Sobhani, H.; Fan, J. A.; Kundu, J.; Capasso, F.; Nordlander, P.; Halas, N. J. Fano Resonances in Plasmonic Nanoclusters: Geometrical and Chemical Tunability. *Nano Lett.* **2010**, *10*, 3184–3189.
24. Cubukcu, E.; Zhang, S.; Park, Y. S.; Bartal, G.; Zhang, X. Split Ring Resonator Sensors for Infrared Detection of Single Molecular Monolayers. *Appl. Phys. Lett.* **2009**, *95*, 043113.
25. Ho, J. F.; Luk'yanchuk, B.; Zhang, J. B. Tunable Fano Resonances in Silver−Silica−Silver Multilayer Nanoshells. *Appl. Phys. A: Mater. Sci. Process.* **2012**, *107*, 133–137.

26. Gallinet, B.; Martin, O. J. F. Relation between Near-Field and Far-Field Properties of Plasmonic Fano Resonances. *Opt. Express* **2011**, *19*, 22167–22175.
27. Hao, F.; Nordlander, P.; Burnett, M. T.; Maier, S. A. Enhanced Tunability and Linewidth Sharpening of Plasmon Resonances in Hybridized Metallic Ring/Disk Nanocavities. *Phys. Rev. B* **2007**, *76*, 245417.
28. Gallinet, B.; Martin, O. J. F. Influence of Electromagnetic Interactions on the Line Shape of Plasmonic Fano Resonances. *ACS Nano* **2011**, *5*, 8999–9008.
29. Verellen, N.; Van Dorpe, P.; Huang, C. J.; Lodewijks, K.; Vandenbosch, G. A. E.; Lagae, L.; Moshchalkov, V. V. Plasmon Line Shaping Using Nanocrosses for High Sensitivity Localized Surface Plasmon Resonance Sensing. *Nano Lett.* **2011**, *11*, 391–397.
30. Zhang, S. P.; Bao, K.; Halas, N. J.; Xu, H. X.; Nordlander, P. Substrate-Induced Fano Resonances of a Plasmonic: Nanocube: A Route to Increased-Sensitivity Localized Surface Plasmon Resonance Sensors Revealed. *Nano Lett.* **2011**, *11*, 1657–1663.
31. Johnson, P. B.; Christy, R. W. Optical-Constants of Noble-Metals. *Phys. Rev. B* **1972**, *6*, 4370–4379.